Available online at www.sciencedirect.com
SCIENCE DIRECT®
Journal of Sound and Vibration 287 (2005) 297–314
JOURNAL OF SOUND AND VIBRATION
www.elsevier.com/locate/jsvi

A spectral super element for modelling of plate vibration. Part 1: general theory

F. Birgersson, S. Finnveden*, C.-M. Nilsson

MWL, Aeronautical and Vehicle Engineering, KTH, SE-100 44 Stockholm, Sweden

Received 15 April 2004; received in revised form 28 October 2004; accepted 3 November 2004
Available online 19 January 2005

Abstract

The dynamic response of vibrating structures is studied with a proposed merger of the standard finite element method with the more computationally efficient spectral finite element method. First a plate structure is modelled with a newly developed spectral super element. Then this element is coupled to other parts that can have a more complex geometry and are modelled entirely with conventional finite elements. Some numerical examples are given to illustrate and validate the developed method and studies of numerical stability are also presented. In an accompanying paper the predicted and measured response of a turbulence excited aircraft panel are compared.

1. Introduction

The finite element method (FEM) provides a mathematically stable environment to simulate dynamic response and it also allows complex geometrical structures to be modelled. However, with high-frequency excitation and distributed random excitation, many structures of interest require impossibly large computer models.

A number of methods to reduce the number of degrees of freedom (dof) and increase the computational efficacy have been presented in the past, for example the spectral finite element

*Corresponding author.
E-mail address: svantef@kth.se (S. Finnveden).

0022-460X/$ - see front matter © 2004 Elsevier Ltd. All rights reserved.
doi:10.1016/j.jsv.2004.11.012

method (SFEM) [1], the transfer matrix method [2], the dynamic stiffness method (DSM) [3,4], the wave-based method [5] and scale-independent elements [6]. These are all formulated in the frequency domain and the frequency-dependent formulation simplifies the inclusion of frequency-dependent material characteristics and boundary condition. The basis functions in these methods are exact or approximate solutions to the local equations of harmonic motion and the elements are assembled as in the standard FEM.

For sub structures that have uniform properties along one direction, say, the x-direction, the local solution on the cross section, i.e. in the yz plane, can conveniently be approximated by polynomial displacement functions. This two-dimensional finite element technique first appeared in Ref. [7] and more recently in references describing wave propagation in laminated composite structures [8,9], thin-walled beams [10,11], rib-stiffened panels [12], anisotropic shells and beams [13,14], fluid-filled pipes [15,16], pre-stressed and curved shells [17] and a wind tunnel [11]. This finite element technique will be referred to here as the waveguide FEM and one of its advantages compared to conventional FEM is that different wave types are readily identified and can be analysed, allowing for a physical understanding of the investigated structure.

This study proposes a new application of the waveguide FEM, where the displacement is described as a combination of found wave solutions. This displacement is then expressed as a function of the nodal displacement at the waveguide ends and inserted in the equation of virtual work. Requiring the first variation of these displacements to be zero, the structural response is found. This method can be seen as a merger of the waveguide FEM with the SFEM and was named spectral super element method (SSEM).

These spectral super elements are characterized by the ease with which they can be put into an assembly with proper coupling to neighbouring elements. Hence, large wave-carrying parts of a structure can be described by this method, whereas smaller parts with complex geometry are modelled entirely by finite elements. In Ref. [3], a super element was created by condensing all the interior dof for a finite element method. Then, the remaining dof were reduced in order to be compatible with the waveguide dof at the joints. With the method presented here such a reduction is not necessary as long as the same nodes are used at the joints with the FEM and SSEM.

A somewhat related finite strip method (FSM) [18,19] also uses polynomial displacement functions to represent the displacement of the cross-section for thin flat-walled structures. This FSM now exists in a number of variants and has been successfully applied to composite laminated structures, e.g. Ref. [20]. However, since the displacement in the direction of the waveguide is described either as a combination of beam eigenfunctions or polynomial spline functions, the FSM leads to a different analysis than with the SSEM. Nevertheless, many application areas for the FSM are most likely also worth studying with the SSEM.

The following is a general theory for a spectral super element. In an accompanying paper [21] distributed excitation is investigated and the element is used to predict the turbulent boundary layer (TBL) response of a clamped plate. Much effort was invested in the validation of the element against similar elements described by either the DSM or the FEM. Two examples of the coupling of spectral super elements to finite elements are provided.

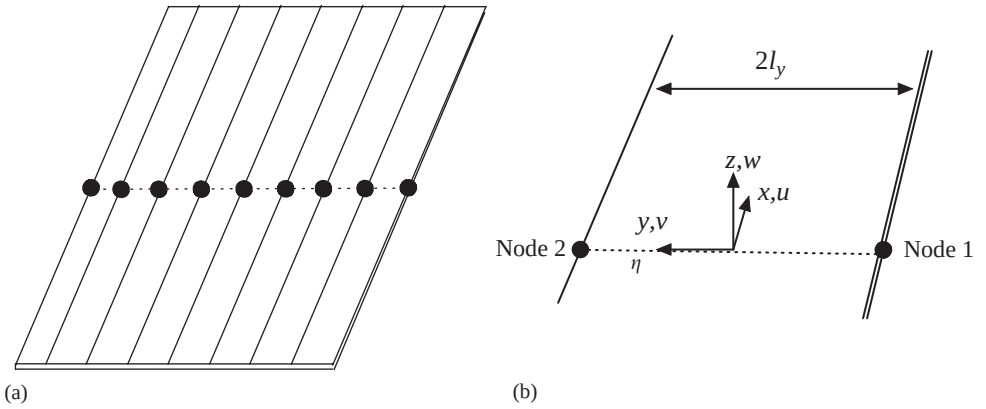

Fig. 1. Plate structure divided into plate strips (a) and single strip element (b).

2. Waveguide formulation

In this section, the equation of motion for a rectangular plate strip, see Fig. 1, will be derived. A plate structure can then be seen as built up from a number of such strips. Uniform properties along the x-direction are assumed in the waveguide formulation described here. For the cross-section in the yz plane, polynomial displacement functions are prescribed, whereas the nodal displacements are here considered functions of x. These displacement functions are used as test functions in a variational approach and thus the equations of motion for the plate strip are found.

2.1. Variational statement

The strain energy of an isotropic thin plate is described in the time domain by for example Ref. [22, pp. 30–35]. For harmonic motion of the form $e^{i\omega t}$, where ω is angular frequency, it is possible to let time stretch from minus infinity to plus infinity and then apply Parseval's identity, see e.g. Ref. [1]. Thus a similar expression for the strain energy is obtained in the frequency domain

$$e_{\text{pot}} = \int\int\int \boldsymbol{\varepsilon}^{*\mathrm{T}} \mathbf{C} \boldsymbol{\varepsilon} \, \mathrm{d}x \, \mathrm{d}y \, \mathrm{d}\omega, \tag{1}$$

where * denotes complex conjugate and $^{\mathrm{T}}$ denotes transpose. $\mathbf{C}$ is the rigidity matrix, which for a homogeneous isotropic plate is given by

$$\mathbf{C} = \begin{pmatrix} \mathbf{C}_0 & \mathbf{0} \\ \mathbf{0} & \frac{h^2}{12}\mathbf{C}_0 \end{pmatrix} \quad \text{with} \quad \mathbf{C}_0 = \begin{pmatrix} \frac{hE}{1-\nu^2} & \frac{\nu hE}{1-\nu^2} & 0 \\ \frac{\nu hE}{1-\nu^2} & \frac{hE}{1-\nu^2} & 0 \\ 0 & 0 & \frac{hE}{2(1+\nu)} \end{pmatrix}. \tag{2}$$

E denotes Young's modulus, h is the thickness of the plate and ν is Poisson's ratio. The vector $\boldsymbol{\varepsilon}$ contains the components of strain, which are linear functionals of the displacement $\mathbf{u}$ and its

spatial derivatives

$$\boldsymbol{\varepsilon} = \left(\frac{\partial u}{\partial x} \quad \frac{\partial v}{\partial y} \quad \frac{\partial u}{\partial y} + \frac{\partial v}{\partial x} \quad \frac{\partial^2 w}{\partial x^2} \quad \frac{\partial^2 w}{\partial y^2} \quad 2\frac{\partial^2 w}{\partial x \partial y} \right)^{\mathrm{T}}, \tag{3}$$

$$\mathbf{u} = (u \; v \; w)^{\mathrm{T}}, \tag{4}$$

where u, v and w are the displacements in the x-, y- and z-directions, respectively.

The integral of the kinetic energy is given on a similar form by

$$e_{\mathrm{kin}} = \int\int\int \omega^2 \rho h \mathbf{u}^{*\mathrm{T}} \mathbf{u} \, \mathrm{d}x \, \mathrm{d}y \, \mathrm{d}\omega, \tag{5}$$

where ρ is the density of the plate.

Hamilton's principle states that the true motion of a system is the one that minimizes the difference between the time integrals of the strain and kinetic energies. For dissipative motion, Hamilton's principle does not apply and instead a modified version is used here, see Refs. [1,23]. The dissipative forces are attributed by a, possibly frequency dependent, complex Young's modulus in Eq. (2). The functional that is minimized for the true motion of the system is found, when the complex conjugates of strain and displacements in Eqs. (1) and (5) are replaced with the complex conjugates of strain and displacement in a mathematically designed adjoint system, which has negative damping. Furthermore, for linear vibrations different frequency components do not couple and, for simplicity, only one frequency is considered at a time. The resulting functional is the Lagrangian L,

$$L = \int\int \boldsymbol{\varepsilon}^{a\mathrm{T}} \mathbf{C} \boldsymbol{\varepsilon} - \omega^2 \rho h \mathbf{u}^{a\mathrm{T}} \mathbf{u} \, \mathrm{d}x \, \mathrm{d}y, \tag{6}$$

where superscript a denotes the complex conjugate of the response variable in the adjoint system. This Lagrangian is minimized for the true motion of the system, subject to the boundary conditions.

2.2. Shape functions

Fig. 1(b) shows a thin strip element with two node points and a width of $2l_y$. There are four dof at each node, namely the three displacement components and the rotation about the x-axis. Since there are all in all eight dof, the shape functions in the y-direction can be represented by polynomials having eight terms, that is

$$u(y) = c_1 + c_2\eta, \quad v(y) = c_3 + c_4\eta, \quad w(y) = c_5 + c_6\eta + c_7\eta^2 + c_8\eta^3, \tag{7}$$

where $\eta = y/l_y$ and c_i are constants. Evaluating these functions as well as the rotation $\delta w/\delta y$ at $\eta = \pm 1$ makes it possible to express the displacements as functions of the nodal dof $\mathbf{V}$

$$u(y) = \mathbf{f}\mathbf{C}_u\mathbf{V}, \quad v(y) = \mathbf{f}\mathbf{C}_v\mathbf{V}, \quad w(y) = \mathbf{f}\mathbf{C}_w\mathbf{V}, \tag{8}$$

where

$$\mathbf{f}(y) = (1 \; \eta \; \eta^2 \; \eta^3), \tag{9}$$

$$\mathbf{V} = (u_1 \; v_1 \; w_1 \; \partial w_1/\partial y \; u_2 \; v_2 \; w_2 \; \partial w_2/\partial y)^{\mathrm{T}}. \tag{10}$$

Indices 1 and 2 denote displacement at nodes 1 and 2, respectively. $\mathbf{C}_{u,v,w}$ are 4×8 matrices with all zero elements except for

$$(\mathbf{C}_u)_{(1,1),(1,5),(2,5)} = \tfrac{1}{2}, \quad (\mathbf{C}_u)_{(2,1)} = -\tfrac{1}{2},$$

$$(\mathbf{C}_v)_{(1,2),(1,6),(2,6)} = \tfrac{1}{2}, \quad (\mathbf{C}_v)_{(2,2)} = -\tfrac{1}{2},$$

$$(\mathbf{C}_w)_{(1,3),(1,7)} = \tfrac{1}{2}, \quad (\mathbf{C}_w)_{(1,4),(3,8),(4,4),(4,8)} = l_y/4, \quad (\mathbf{C}_w)_{(1,8),(2,4),(2,8),(3,4)} = -l_y/4,$$

$$(\mathbf{C}_w)_{(2,3)} = -\tfrac{3}{4}, \quad (\mathbf{C}_w)_{(2,7)} = \tfrac{3}{4}, \quad (\mathbf{C}_w)_{(4,3)} = \tfrac{1}{4}, \quad (\mathbf{C}_w)_{(4,7)} = -\tfrac{1}{4}. \tag{11}$$

2.3. Evaluation of strain and kinetic energies

The shape functions have been derived for a strip element, see Eq. (8). Given the assumption that the geometry in the x-direction is constant, the nodal displacements $\mathbf{V}$ can be considered as functions of x. With these shape functions it is possible to rewrite the terms $\boldsymbol{\varepsilon}$ and $\mathbf{u}$ in Eqs. (3) and (4) as follows:

$$\boldsymbol{\varepsilon} = \boldsymbol{\varepsilon}_0 \mathbf{V}(x) + \boldsymbol{\varepsilon}_1 \frac{\partial \mathbf{V}(x)}{\partial x} + \boldsymbol{\varepsilon}_2 \frac{\partial^2 \mathbf{V}(x)}{\partial x^2}, \quad \mathbf{u} = \mathbf{u}_0 \mathbf{V}(x), \tag{12}$$

where

$$\boldsymbol{\varepsilon}_0 = \begin{pmatrix} \mathbf{0} \\ \mathbf{f}'\mathbf{C}_v \\ \mathbf{f}'\mathbf{C}_u \\ \mathbf{0} \\ \mathbf{f}''\mathbf{C}_w \\ \mathbf{0} \end{pmatrix}, \quad \boldsymbol{\varepsilon}_1 = \begin{pmatrix} \mathbf{f}\mathbf{C}_u \\ \mathbf{0} \\ \mathbf{f}\mathbf{C}_v \\ \mathbf{0} \\ \mathbf{0} \\ 2\mathbf{f}'\mathbf{C}_w \end{pmatrix}, \quad \boldsymbol{\varepsilon}_2 = \begin{pmatrix} \mathbf{0} \\ \mathbf{0} \\ \mathbf{0} \\ \mathbf{f}\mathbf{C}_w \\ \mathbf{0} \\ \mathbf{0} \end{pmatrix}, \quad \mathbf{u}_0 = \begin{pmatrix} \mathbf{f}\mathbf{C}_u \\ \mathbf{f}\mathbf{C}_v \\ \mathbf{f}\mathbf{C}_w \end{pmatrix}. \tag{13}$$

Prime denotes differentiation with respect to y. Inserting these expressions in Lagrangian (6) yields

$$L^s = \int \sum_{m=0}^{2} \sum_{n=0}^{2} \frac{\partial^m \mathbf{V}^{a\mathrm{T}}}{\partial x^m} \boldsymbol{\varepsilon}^s_{mn} \frac{\partial^n \mathbf{V}}{\partial x^n} - \omega^2 \mathbf{V}^{a\mathrm{T}} \mathbf{m}^s_{00} \mathbf{V} \, \mathrm{d}x, \tag{14}$$

where

$$\boldsymbol{\varepsilon}^s_{mn} = \int_{-l_y}^{l_y} \boldsymbol{\varepsilon}_m^{\mathrm{T}} \mathbf{C} \boldsymbol{\varepsilon}_n \, \mathrm{d}y, \quad \mathbf{m}^s_{00} = \rho h \int_{-l_y}^{l_y} \mathbf{u}_0^{\mathrm{T}} \mathbf{u}_0 \, \mathrm{d}y. \tag{15}$$

$\boldsymbol{\varepsilon}^s_{mn}$ and $\mathbf{m}^s_{00}$ are 8×8 matrices. The derivatives and integrals with respect to y in Eq. (15) are evaluated exactly, either with Gauss integration or analytically, cf. Refs. [10,12]. The Lagrangian is so far only evaluated for a single strip element, which is stressed by the superscript s.

2.3.1. Assembling and imposing boundary conditions

To evaluate the strain and kinetic energies for an assembly of plate strips a Lagrangian is formulated for each strip. The final Lagrangian, here denoted L, consists of $\boldsymbol{\varepsilon}_{mn}$ and $\mathbf{m}_{00}$, which are square matrices of size four times the number of nodes in the assembled structure. These matrices are assembled similar to a conventional finite element method, where the strip elements are transformed to the global coordinate system. The Lagrangian can thus be written as

$$L = \int \sum_{m=0}^{2} \sum_{n=0}^{2} \frac{\partial^m \mathbf{V}^{a\mathrm{T}}}{\partial x^m} \boldsymbol{\varepsilon}_{mn} \frac{\partial^n \mathbf{V}}{\partial x^n} - \omega^2 \mathbf{V}^{a\mathrm{T}} \mathbf{m}_{00} \mathbf{V} \, \mathrm{d}x, \tag{16}$$

where $\boldsymbol{\varepsilon}_{mn}$ and $\mathbf{m}_{00}$ have been assembled and are symmetric banded matrices.

Boundary conditions are imposed similar to conventional FEM, i.e. nodal dof of $\mathbf{V}$ are restrained by simply constraining the appropriate rows and columns of $\boldsymbol{\varepsilon}_{mn}$ and $\mathbf{m}_{00}$. For a simply supported edge on one side, for example, the three first rows and columns would be constrained.

2.4. Equations of motion

The equations of motion are found from Eq. (16) with the calculus of variation as

$$\left(\mathbf{A}_4 \frac{\partial^4}{\partial x^4} + \mathbf{A}_2 \frac{\partial^2}{\partial x^2} + \mathbf{A}_1 \frac{\partial}{\partial x} + \mathbf{A}_0 - \omega^2 \mathbf{M} \right) \mathbf{V}(x) = \mathbf{0}, \tag{17}$$

where

$$\mathbf{A}_4 = \boldsymbol{\varepsilon}_{22}, \quad \mathbf{A}_2 = \boldsymbol{\varepsilon}_{02} - \boldsymbol{\varepsilon}_{11} + \boldsymbol{\varepsilon}_{20}, \quad \mathbf{A}_1 = \boldsymbol{\varepsilon}_{01} - \boldsymbol{\varepsilon}_{10}, \quad \mathbf{A}_0 = \boldsymbol{\varepsilon}_{00}, \quad \mathbf{M} = \mathbf{m}_{00}. \tag{18}$$

$\mathbf{A}_3$ turns out to be zero for the investigated element and is not included. For curved shell elements it is non-zero [17] and needs to be accounted for. For reasons of symmetry, the same equation of motion can be derived for the adjoint system.

2.4.1. Wave solutions and wavenumbers

For a given frequency, Eq. (17) is a set of coupled ordinary differential equations with constant coefficients. Its solutions are therefore given by exponential functions and a polynomial eigenvalue problem follows. This problem is then transformed to a standard linear eigenvalue problem, see for example Refs. [12,24], with solutions of the form

$$\mathbf{V}(x) = \boldsymbol{\Phi} \mathbf{E}(x) \mathbf{a}, \tag{19}$$

where $\mathbf{a}$ are wave amplitudes and the entries of the diagonal matrix $\mathbf{E}$ are given by

$$(\mathbf{E})_{ii} = \mathrm{e}^{\kappa_{ii} x - (\kappa_p)_{ii} l_x}, \tag{20}$$

where $\boldsymbol{\kappa}$ is a diagonal matrix of eigenvalues. To each component κ_{ii} the ith column of $\boldsymbol{\Phi}$ gives the corresponding eigenvector. The wave expressions are scaled for reasons of numerical stability by factors $\mathrm{e}^{(\kappa_p)_{ii} l_x}$, where l_x is half the length of the plate to be investigated and

$$(\kappa_p)_{ii} = \kappa_{ii}, \ \ \mathrm{Re}(\kappa_p)_{ii} \geqslant 0; \quad \text{else } (\kappa_p)_{ii} = -\kappa_{ii}. \tag{21}$$

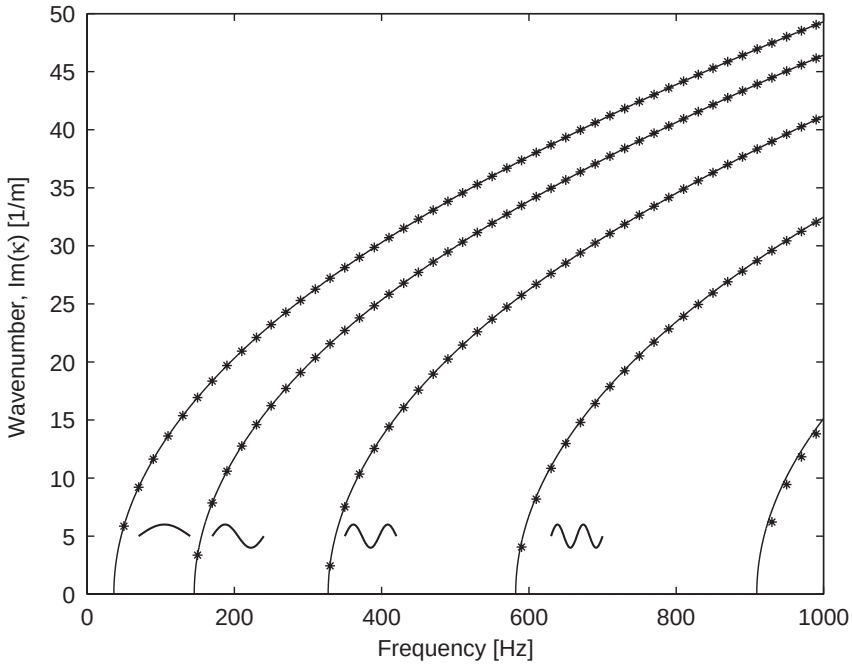

Fig. 2. Dispersion curves of simply supported plate. Transverse mode shapes are shown next to the curves. ⋆, using 9 assembled element strips for the waveguide formulation; solid, analytical solution.

Table 1
Relative error of predicted wavenumber for plate strip in Fig. 2 at 800 Hz

Transverse mode n	Number of strip elements		
	3	9	18
1	1.67e − 6	1.22e − 8	6.80e − 10
2	3.62e − 4	3.52e − 6	2.13e − 7
3	1.94e − 2	1.19e − 4	7.48e − 6
4	2.07e − 1	2.37e − 3	1.60e − 4

The eigenvalues κ_{ii}, here also referred to as wavenumbers, are solved numerically for a given frequency once the equations of motion have been assembled. In Fig. 2 the case of a simply supported plate is investigated. The resulting dispersion curves using nine strip elements are shown, where the material characteristics and geometry of the plate are given in Section 4.1. No damping was used here and the known analytical wavenumbers for flexural waves, e.g. Ref. [3], are shown as comparison. The analytical and predicted dispersion curves agree very well and with more elements the relative error of the predicted wavenumbers decreased; a selected study of convergence is shown in Table 1 for the four first-order transverse modes.

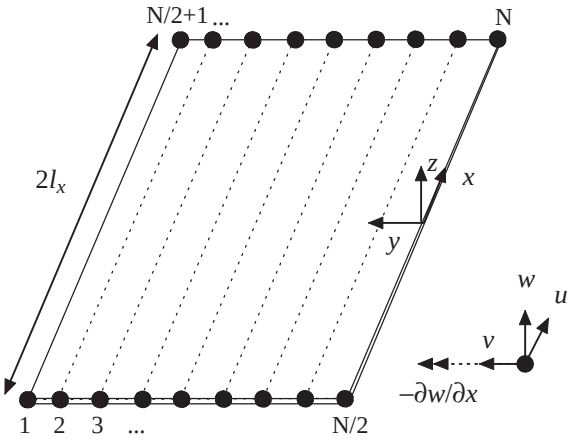

Fig. 3. Geometry of rectangular element with nodes. Shown with dotted lines are the plate strips used to find the basis functions. Shown to the right are the nodal dof.

3. Spectral super element formulation

In this section the dynamic stiffness matrix for a rectangular plate element will be derived. The wave solutions found in the previous section are used as basis functions for a variational principle. Similar to a conventional finite element method, the dof are the nodal displacements at the nodes, see Fig. 3. Experience has shown that it is not always possible to project the wave solutions on the nodal dof and in order to gain numerical stability a dynamic condensation and a weighted least-square procedure are proposed here.

3.1. Element displacement functions

The wave solutions, $\mathbf{V}(x) = \mathbf{\Phi E}(x)\mathbf{a}$, derived in the previous section will be used to describe the displacement. Now, suppose that at the nodes the displacements $\mathbf{W}_i$ are prescribed

$$\mathbf{B}_1\mathbf{V}(-l_x) = \mathbf{W}_1, \quad \mathbf{B}_2\frac{\partial \mathbf{V}(-l_x)}{\partial x} = \mathbf{W}_2,$$

$$\mathbf{B}_3\mathbf{V}(+l_x) = \mathbf{W}_3, \quad \mathbf{B}_4\frac{\partial \mathbf{V}(+l_x)}{\partial x} = \mathbf{W}_4, \tag{22}$$

where $\mathbf{B}_i$ are matrices consisting of rows, each filled with zeros except for one entry that is unity in order to select the dof to be restricted. From Eq. (22) it is possible to solve the wave amplitudes $\mathbf{a}$ as functions of the prescribed nodal displacements and thus write the displacement functions as

$$\mathbf{V}(x) = \mathbf{\Phi E}(x)\mathbf{AW}, \tag{23}$$

where **A** is found from solving the system

$$\mathbf{BA} = \mathbf{I} \quad \text{with } \mathbf{B} = \begin{pmatrix} \mathbf{B}_1\mathbf{\Phi}\mathbf{E}(-l_x) \\ \mathbf{B}_2\mathbf{\Phi}\kappa\mathbf{E}(-l_x) \\ \mathbf{B}_3\mathbf{\Phi}\mathbf{E}(+l_x) \\ \mathbf{B}_4\mathbf{\Phi}\kappa\mathbf{E}(+l_x) \end{pmatrix}, \quad \mathbf{W} = \begin{pmatrix} \mathbf{W}_1 \\ \mathbf{W}_2 \\ \mathbf{W}_3 \\ \mathbf{W}_4 \end{pmatrix}. \tag{24}$$

I is an identity matrix of appropriate dimensions. Often, many dof are used in order to obtain the wave solutions. Then, similar to a modal substructuring, only a few dof are used in the global model. Thus the number of waves is greater than the number of prescribed boundary conditions, i.e. vector **a** has more components than vector **W**. This in turn means that the system is underdetermined and there are infinitely many solutions. If not otherwise stated, this system is solved here in a least-squares sense to the underdetermined system (see command '\' in MATLAB). The effective rank B of **B** is determined from an orthogonal–triangular decomposition with pivoting and a solution for **A** is computed which has at most B non-zero components per column.

If it was possible, when deciding among the available wave solutions from which to find the true displacement of the plate, to select those wave solutions that are the most likely to contribute to this displacement, then the predictions would become more accurate. With this knowledge, it is natural to sort the waves according to their transverse mode shapes and then neglect the highest order mode shapes and possibly also the ones that are not excited by the force. These higher order mode shapes are usually not accurate as they will have less or close to two nodes per wavelength. The sampling theorem tells us that these waves will then look similar at the nodes to lower order waves and sometimes they replaced lower order waves, when projecting the wave solutions onto the nodal dof. This in turn resulted in a decrease in accuracy that was noticeable especially at very low frequencies.

In light of the previous discussion three approaches were used in this paper in order to find matrix **A**.

- *Straightforward approach*: All waves found were used.
- *Weighted least-squares approach*: All eigenvectors, described by the columns of $\mathbf{\Phi}$, were scaled to have an L2-norm equal to $1/|\kappa_{ii}|^2$, where κ_{ii} is the corresponding wavenumber to each eigenvector. In this way an important weighting function is introduced, before the system of equations (24) is solved with a least-squares method. Wave solutions that have large wavenumbers, describing a rapid decay, will become discriminated, when projecting the solutions onto the nodal dof. Instead solutions with small wavenumbers, corresponding to waves that have cut on or are about to cut on, will be chosen to describe the displacement of the plate, thereby encouraging the solution to follow Saint-Venant's principle [25].
- *Dynamic condensation approach*: A reduced set of waves were used in combination with a dynamic condensation procedure presented in Appendix A. The main idea behind this is that instead of solving an underdetermined system in a least-squares sense to find **A**, the virtual work at the boundary is included in the Lagrangian. This results in a new system of equations that can be solved by Gaussian elimination alone.

The difference in predicted response with these three methods is commented on in the section with numerical results.

3.2. Dynamic stiffness matrix

The element displacement functions are now described by Eq. (23) and from symmetry of the bi-linear Lagrangian the complex conjugate of the displacement functions for the adjoint system are similarly given by

$$\mathbf{V}^a(x) = \mathbf{\Phi}\mathbf{E}(x)\mathbf{A}\mathbf{W}^a. \tag{25}$$

Substituting these displacement functions into Lagrangian (16) yields

$$L = \int_{-l_x}^{l_x} \sum_{m=0}^{2}\sum_{n=0}^{2} \mathbf{W}^{a\mathrm{T}}\mathbf{A}^{\mathrm{T}} \frac{\partial^m \mathbf{E}(x)^{\mathrm{T}}}{\partial x^m} \mathbf{\Phi}^{\mathrm{T}} \boldsymbol{\varepsilon}_{mn} \mathbf{\Phi} \frac{\partial^n \mathbf{E}(x)}{\partial x^n} \mathbf{A}\mathbf{W} - \omega^2 \mathbf{W}^{a\mathrm{T}}\mathbf{A}^{\mathrm{T}}\mathbf{E}(x)^{\mathrm{T}}\mathbf{\Phi}^{\mathrm{T}}\mathbf{m}_{00}\mathbf{\Phi}\mathbf{E}(x)\mathbf{A}\mathbf{W}\,\mathrm{d}x, \tag{26}$$

where the identity $(\mathbf{v}_1\mathbf{v}_2)^{\mathrm{T}} = \mathbf{v}_2^{\mathrm{T}}\mathbf{v}_1^{\mathrm{T}}$ was used. Note that the mth derivative of the diagonal matrix $\mathbf{E}(x)$ is another diagonal matrix $\kappa^m\mathbf{E}(x)$. For two diagonal matrices $\mathbf{d}_1$ and $\mathbf{d}_2$ and another arbitrary matrix $\mathbf{v}$ of appropriate dimension the following holds:

$$\mathbf{d}_1\,\mathbf{v}\,\mathbf{d}_2 = \mathbf{v}.*(\mathrm{diag}(\mathbf{d}_1)\mathrm{diag}(\mathbf{d}_2)^{\mathrm{T}}), \tag{27}$$

where the operator diag produces a column vector from its argument's main diagonal and $.*$ denotes element wise multiplication (as in MATLAB). Using identity (27), Lagrangian (26) can be rewritten as

$$L = \mathbf{W}^{a\mathrm{T}}\mathbb{D}\mathbf{W}, \tag{28}$$

where the dynamic stiffness matrix $\mathbb{D}$ is given by

$$\mathbb{D} = \mathbf{A}^{\mathrm{T}}(\mathbf{\Theta}.*\mathbf{E}_{\mathbf{I}})\mathbf{A}, \tag{29}$$

$$\mathbf{\Theta} = \left(\sum_{m=0}^{2}\sum_{n=0}^{2}(\kappa^m(\mathbf{\Phi}^{\mathrm{T}}\boldsymbol{\varepsilon}_{mn}\mathbf{\Phi})\kappa^n) - \omega^2(\mathbf{\Phi}^{\mathrm{T}}\mathbf{m}_{00}\mathbf{\Phi})\right), \tag{30}$$

$$\mathbf{E}_{\mathbf{I}} = \int_{-l_x}^{l_x} (\mathrm{diag}\mathbf{E}(x))(\mathrm{diag}\mathbf{E}(x))^{\mathrm{T}}\,\mathrm{d}x. \tag{31}$$

The integral in Eq. (31) is solved analytically and consequently the entries of the matrix generating function $\mathbf{E}_{\mathbf{I}}$ are given by

$$(\mathbf{E}_{\mathbf{I}})_{ij} = ((\mathrm{e}^{\kappa_{ii}(+l_x)-(\kappa_p)_{ii}l_x})(\mathrm{e}^{\kappa_{jj}(+l_x)-(\kappa_p)_{jj}l_x}) - (\mathrm{e}^{\kappa_{ii}(-l_x)-(\kappa_p)_{ii}l_x})(\mathrm{e}^{\kappa_{jj}(-l_x)-(\kappa_p)_{jj}l_x}))/((\kappa)_{ii}+(\kappa)_{jj}). \tag{32}$$

With the scaling introduced in Eq. (20) this expression can be evaluated for large κ and a Taylor expansion was applied for small values of $\kappa_{ii}+\kappa_{jj}$.

The dynamic stiffness matrix (29) does not depend on the excitation of the structure. An arbitrary forcing $\mathbf{p}$ can be considered by the inclusion of the virtual work of this force in the

Lagrangian, as in Refs. [1,26],

$$L_f = \int_{-l_x}^{l_x} \int_{-l_y}^{l_y} -\mathbf{p}^{*\mathrm{T}}\mathbf{u} - \mathbf{u}^{a\mathrm{T}}\mathbf{p}\,\mathrm{d}y\,\mathrm{d}x = -\mathbf{F}^{*\mathrm{T}}\mathbf{W} - \mathbf{W}^{a\mathrm{T}}\mathbf{F}, \tag{33}$$

where $\mathbf{F}$ is a generalized force vector. In this paper only point forces at node locations are considered and the integral is then trivial to evaluate. However, for distributed excitation, as shown in an accompanying paper, a particular solution to the non-homogeneous equations of motion has to be included in the formulation and the above integral has to be calculated explicitly [21]. Requiring the first variation with respect to the nodal displacements of the adjoint system $\mathbf{W}^a$ to be zero in Eqs. (28) and (33), a system of equations for the nodal displacement $\mathbf{W}$ is found

$$\mathbb{D}\mathbf{W} = \mathbf{F}. \tag{34}$$

Solving Eq. (34) gives the nodal displacements $\mathbf{W}$ and from Eqs. (8) and (23) the displacement of the structure at any position is given.

3.3. Coupling with conventional finite elements

It is convenient to model small and geometrically complicated parts of a structure with conventional finite elements. Assuming harmonic motion, the dynamic stiffness matrix is

$$\mathbb{D} = \mathbf{K}^{\mathrm{FEM}} - \omega^2\mathbf{M}^{\mathrm{FEM}}, \tag{35}$$

where $\mathbf{M}^{\mathrm{FEM}}$ is the inertia matrix and $\mathbf{K}^{\mathrm{FEM}}$ is the stiffness matrix. These are described, for example, in Ref. [22]. To couple a spectral super element with conventional finite elements, the shared nodal dof are set equal making the assembly process the same as for conventional finite elements. However, since there are no nodes along two sides of the structure, these sides cannot be coupled this way.

4. Validation

4.1. Investigated structures

Two different plate structures will be investigated here, described below as test cases (a) and (b). Both these structures had a length L_x of 76.8 cm and a width L_y of 32.8 cm, a Young's modulus E of $7 \times 10\,\mathrm{N/m^2}$, a density of $2700\,\mathrm{kg/m^3}$ and a Poisson ratio of 0.33. Damping was modelled with a complex Young's modulus $E(1 + \mathrm{i}\eta)$, where η was 0.02. Fig. 4(a) and (b) show the geometry for these two test cases. The global coordinate system has its origin in the lower left corner of the respective structures.

In test case (a), the plate consisted of two coupled plates. Plate 1 had a thickness h of 1.6 mm and a length of $2L_x/3$, whereas plate 2 had a thickness of 3.2 mm and a length of $L_x/3$. A vertical point force exciting only flexural waves was applied at $(x = 2L_x/3, y = 5L_y/9)$ and the response was calculated at $(x = 28L_x/57, y = 4L_y/9)$. Two opposite sides of the plate structure were simply supported and the other two clamped. The main reason for studying this case was the fact that there exists an analytical solution given for example by a spectral finite element method or a

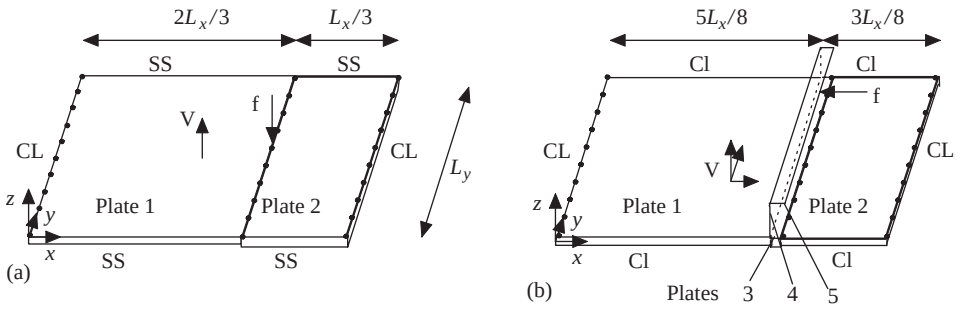

Fig. 4. Geometry of the two plate structures used for validation. Each structure consisted of two connected plates, where the second structure also had a stringer attached to it consisting of three plates. SS and CL denotes simply supported and clamped edges, respectively.

dynamic stiffness method, see Ref. [27]. Against this solution three different methods could be tested for accuracy and efficiency:

- A spectral super element method with one element for each plate (SSEM).
- A spectral super element for plate 1 coupled to a finite element method for plate 2 (SSEM–FEM).
- A finite element method to model both plates (FEM).

Ten nodes were used in the y-direction for both the SSEM and the FEM and it was therefore easy to couple the two methods. For the FEM, plate 1 was modelled with 10×20 nodes and plate 2 with 10×10 nodes, i.e. all in all 252 elements as compared to two elements with the SSEM. The non-conforming finite element that was used for the plate is often referred to as ACM element and is described in for example Ref. [22, Chapters 4.2 and 6.1].

In test case (b), the investigated structure consisted of five plate structures, see Fig. 4(b). These were all modelled with 19 transverse nodes in order to make it easy to couple all plates. The stringer was modelled entirely with finite elements; plates three, four and five consisted of 19×4, 19×4 and 19×3 nodes, respectively. Plates 1 and 2 were modelled either with finite elements (FEM) or with spectral super elements coupled with the finite elements of the stringer (SSEM–FEM). The number of nodes and elements were increased with a factor four compared to test case (a) in order to reduce the error of the FEM, i.e. approximately 1000 finite elements or 2 superspectral elements. All plates had a thickness h of 1.6 mm, except for plate 3 with a thickness of 3.2 mm. The length of plates 1–5 was 480, 280, 8, 28 and 10 mm, respectively. A horizontal point force was applied at the free edge of plate 5 with $(y = 7L_y/9)$, and the response was calculated at plate 1 with $(x = 35L_x/76, y = 5L_y/9)$.

4.2. Numerical results

Fig. 5 compares the transfer mobility for test case (a). Up to approximately 400 Hz all methods agree well with the analytical solution. Then the FEM starts to become erroneous and soon after

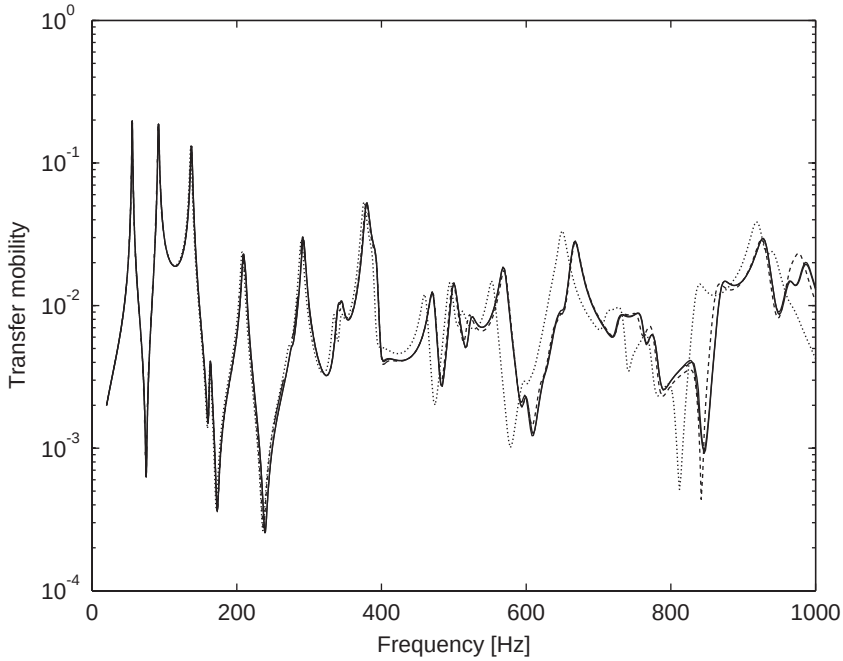

Fig. 5. Transfer mobility for test case a. Solid line, analytical and equally SSEM; dashed, SSEM–FEM; dotted, FEM.

the method, where one spectral super element is coupled to finite elements (SSEM–FEM) also starts to show large errors. Around this frequency the third transverse mode cuts on, see Fig. 2, and thus there will be less than six nodes per structural wavelength. The best method is the SSEM, which stays quite accurate also at frequencies well above 1000 Hz, i.e. even after the fourth- and fifth-order transverse modes have cut on. Hence, the SSEM seems to be more forgiving than the FEM, if less transverse nodes are used per structural wavelength. Furthermore, the number of dof was reduced with the SSEM by a factor 27, from 972 down to 36, as compared to the FEM. Fig. 6 shows the relative error in the predicted transfer mobility averaged over third octave bands. The relative error of the SSEM is almost a factor 100 lower than the one for the FEM. The SSEM–FEM was an improvement compared to the FEM, mainly due to the fact that the smallest and thickest element was modelled with the FEM. If ever more of the structure is modelled with the finite elements, then naturally the error will increase. The cost to mesh the smaller element slightly finer is not too expensive, however, and thereby the error can be reduced quite significantly.

At very low frequencies the relative error suddenly starts to increase with the SSEM. Analysis showed that the reason for this is that most waves in the structure, found from solving the equations of motion, are non-propagating at this frequency. It is then difficult to solve Eq. (21) for **A** without some numerical conditioning. This problem was mentioned in Section 3.1 along with two approaches to handle it, i.e. a weighted least-squares and a dynamic condensation approach. Fig. 7 shows the relative error with the weighted least-squares approach compared to the

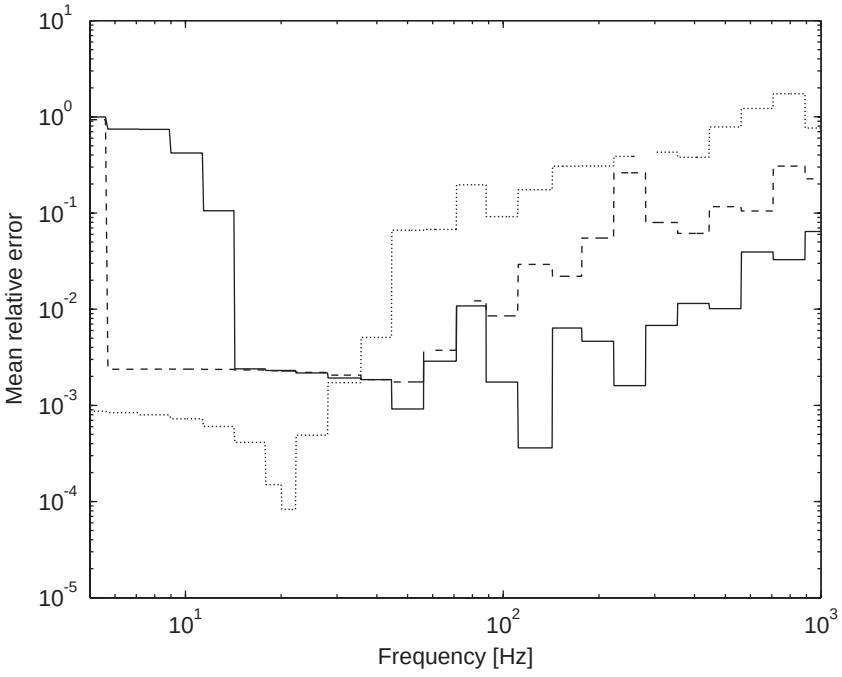

Fig. 6. Relative error in predicted transfer mobility from Fig. 5, averaged over third octave bands. Solid, SSEM without weighting; dashed, SSEM–FEM; dotted, FEM.

straightforward approach. As can be seen the main difference occurs at low frequencies, where a great improvement in accuracy was obtained with the weighted least-squares approach. If the number of transverse nodes was increased, the relative error decreased and the figure shows how this error would decrease by about a factor of 10 if the number of nodes were doubled.

The dynamic condensation approach gave a similar improvement and is not shown. Whenever waves were removed with the dynamic condensation approach, it was important to keep the right amount to ensure enough independent waves to project on the nodal dof. Failure to do so resulted in numerical instability. On the other hand with too few removed the approach sometimes had no effect at all. Therefore, the weighted least-squares approach seemed advantageous for the test cases studied in this paper and from now on all predictions are made with this approach unless stated otherwise.

Figs. 8 and 9 compare the transfer mobility for test case (b). The response was calculated using either a FEM or a SSEM coupled with a FEM, see Section 4.1. Fig. 8 compares the out-of-plane response from the horizontal point force on the stringer and shows a very good agreement between FEM and SSEM–FEM. However, if all waves found from solving the equations of motion are used without any weighting, the SSEM becomes unstable at certain frequencies. Fig. 9 compares the in-plane response from the same point force and shows a similar good agreement.

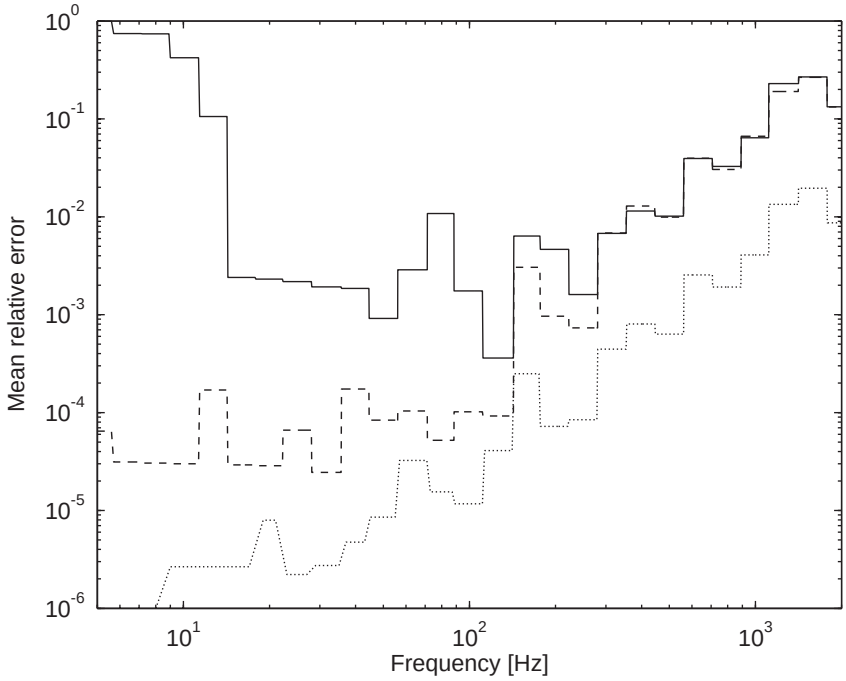

Fig. 7. Relative error in predicted transfer mobility averaged over third octave bands for the SSEM. Solid, SSEM without weighting; dashed, SSEM with weighting; dotted, SSEM with weighting and twice the number of nodes.

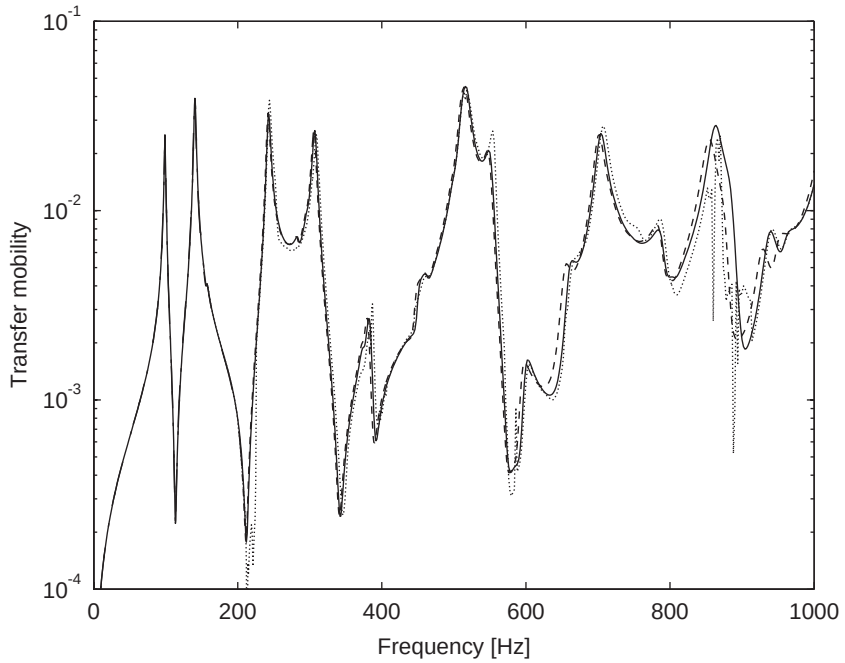

Fig. 8. Transfer mobility for test case b. Out-of-plane velocity due to horizontal point force on stringer. Solid, SSEM–FEM; dashed, FEM; dotted, SSEM–FEM without weighting or reduction of waves.

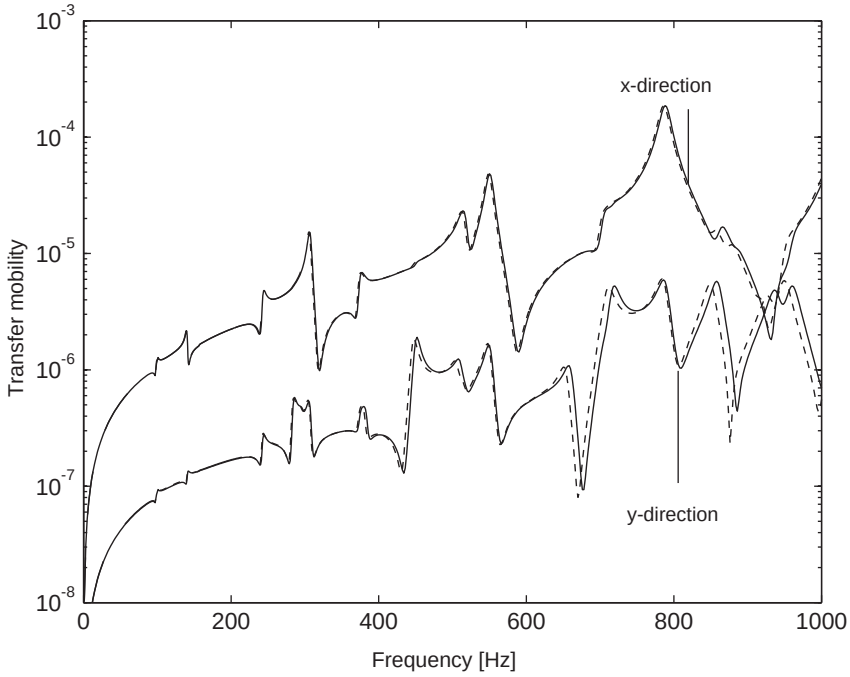

Fig. 9. Transfer mobility for test case b. In-plane velocity in x- and y-direction due to horizontal point force on stringer. Solid, SSEM–FEM; dashed, FEM.

5. Conclusion

A new spectral super element for the analysis of structural vibration at high frequencies has been presented. It describes the motion as a combination of travelling and decaying waves along the structure. These waves are given by a waveguide finite element model, which is versatile and efficient. A major difficulty was to project these waves onto the nodal dof at the element ends and thus select which waves to use when describing the motion of the element. This difficulty was overcome by employing either a weighted least squares or a dynamic condensation approach.

The developed element is useful for structures that are uniform along a single coordinate axis but otherwise arbitrary in material composition and geometry. With the SSEM a considerable reduction in dof can be achieved, which provides increased computational efficiency. Furthermore, since the SSEM has compact support and is formulated in terms of the nodal displacements at the ends, it can easily be coupled to a conventional finite element method. In an accompanying paper the element will be used to predict the response to a turbulence excited aircraft panel [21].

Acknowledgements

This work was supported by the European Commission, ENABLE (GRD4_CT-00-00223) and the Swedish Research Council (621-2002-5661).

Appendix A. Dynamic condensation

To improve the numerical stability, when projecting the wave amplitudes on the nodal dof, an alternative way to formulate the dynamic stiffness matrix will be outlined here. The virtual work at the boundary will be included in the Lagrangian and thus the wave amplitudes are solved as functions of the nodal displacements.

Restraints (22) are included into the variational formulation using Lagrange multipliers and the following terms are added to Lagrangian (16):

$$L_B = \boldsymbol{\lambda}^{a\mathrm{T}}(\mathbf{B}\mathbf{a} - \mathbf{W}) + (\mathbf{B}\mathbf{a}^a - \mathbf{W}^a)^{\mathrm{T}}\boldsymbol{\lambda}, \tag{A.1}$$

where the components of $\boldsymbol{\lambda}$ and $\boldsymbol{\lambda}^a$ are Lagrange multipliers. The wave solutions are still expressed as functions of the unknown wave amplitudes $\mathbf{a}$, see Eq. (19). The functional is now given by $L + L_B$ and it is stationary for the true motion of the structure subject to restraints (22). Thus upon taking the first variation of $\mathbf{a}^a$ and $\boldsymbol{\lambda}^a$, the following set of equations results:

$$\begin{pmatrix} (\boldsymbol{\Theta}.*\mathbf{E}_\mathbf{I}) & \mathbf{B}^{\mathrm{T}} \\ \mathbf{B} & \mathbf{0} \end{pmatrix} \begin{pmatrix} \mathbf{a} \\ \boldsymbol{\lambda} \end{pmatrix} = \begin{pmatrix} \mathbf{0} \\ \mathbf{W} \end{pmatrix}. \tag{A.2}$$

From Eq. (A.2) the wave amplitudes can be solved, if it is successively required that one entry of $\mathbf{W}$ is unity and all other entries are zero. Thus the displacement functions for any nodal displacement $\mathbf{W}$ can be written as

$$\mathbf{V}(x) = \boldsymbol{\Phi}\mathbf{E}(x)\mathbf{A}_\mathbf{d}\mathbf{W}, \tag{A.3}$$

where $\mathbf{A}_\mathbf{d}$ is found from solving the system

$$\begin{pmatrix} (\boldsymbol{\Theta}.*\mathbf{E}_\mathbf{I}) & \mathbf{B}^{\mathrm{T}} \\ \mathbf{B} & \mathbf{0} \end{pmatrix} \begin{pmatrix} \mathbf{A}_\mathbf{d} \\ \boldsymbol{\Lambda} \end{pmatrix} = \begin{pmatrix} \mathbf{0} \\ \mathbf{I} \end{pmatrix}, \tag{A.4}$$

and is given explicitly as

$$\mathbf{A}_\mathbf{d} = (\boldsymbol{\Theta}.*\mathbf{E}_\mathbf{I})^{-1}\mathbf{B}^{\mathrm{T}}(\mathbf{B}(\boldsymbol{\Theta}.*\mathbf{E}_\mathbf{I})^{-1}\mathbf{B}^{\mathrm{T}})^{-1}\mathbf{I}. \tag{A.5}$$

$\mathbf{I}$ is an identity matrix of appropriate dimensions. The same procedure applies also for the adjoint system and, if these newly found displacement functions are inserted in Lagrangian (16), the following dynamic stiffness matrix results

$$\mathbb{D} = \mathbf{A}_\mathbf{d}^{\mathrm{T}}(\boldsymbol{\Theta}.*\mathbf{E}_\mathbf{I})\mathbf{A}_\mathbf{d}, \tag{A.6}$$

where $\boldsymbol{\Theta}.*\mathbf{E}_\mathbf{I}$ is the same as before, see Eqs. (30)–(32).

References

[1] S. Finnveden, Exact spectral finite element analysis of stationary vibrations in a rail way car structure, *Acta Acustica* 2 (1994) 461–482.

[2] Y.K. Lin, B.K. Donaldson, A brief survey of transfer matrix techniques with special reference of aircraft panels, *Journal of Sound and Vibration* 10 (1969) 103–143.

[3] J.F. Doyle, *Wave Propagation in Structures*, Springer, New York, 1997.

[4] A.Y.T. Leung, Dynamic stiffness for structures with distributed deterministic or random loads, *Journal of Sound and Vibration* 242 (3) (2001) 377–395.
[5] W. Desmet, A Wave Based Prediction Technique for Coupled Vibro-Acoustic Analysis, PhD Thesis, K. U. Leuven, division PMA, 1998.
[6] M.M. Ettouney, R.P. Daddazio, N.N. Abboud, Some practical applications of the use of scale independent elements for dynamic analysis of vibrating systems, *Computers and Structures* 65 (3) (1997) 423–432.
[7] B. Aalami, Waves in prismatic guides of arbitrary cross section, *Journal of Applied Mechanics* 40 (1973) 1067–1072.
[8] M. Aberg, Wave Propagation and Damage in Composite Laminates, PhD Thesis, Solid Mechanics, KTH, 1999.
[9] S.K. Datta, A.H. Shah, R.L. Bratton, T. Chakraborty, Wave propagation in laminated composite plates, *Journal of the Acoustical Society of America* 83 (1988) 2002–2026.
[10] L. Gavric, Finite element computation of dispersion properties of thin-walled waveguides, *Journal of Sound and Vibration* 173 (1994) 113–124.
[11] S. Finnveden, Evaluation of modal density and group velocity by a finite element method, *Journal of Sound and Vibration* 273 (2004) 51–75.
[12] U. Orrenius, S. Finnveden, Calculation of wave propagation in rib-stiffened plate structures, *Journal of Sound and Vibration* 198 (1996) 203–224.
[13] T. Mazuch, Wave dispersion in anisotropic shells and rods by the finite element method, *Journal of Sound and Vibration* 198 (1996) 429–438.
[14] V.V. Volovoi, D.H. Hodges, V.L. Berdichevsky, V.G. Sutyrin, Dynamic dispersion curves for non-homogenous anisotropic beams with cross-section of arbitrary geometry, *Journal of Sound and Vibration* 215 (1998) 1101–1120.
[15] A. Bocquillet, Méthode énergétique de caractéeisations vibroacoustiques des résaux complexes, PhD Thesis, Ecole Centrale de Lyon, 2000.
[16] S. Finnveden, Spectral finite element analysis of the vibration of straight fluid-filled pipes with flanges, *Journal of Sound and Vibration* 199 (1997) 125–154.
[17] C.-M. Nilsson, Waveguide Finite Elements for Thin-walled Structures, Lic. Thesis, MWL, KTH, TRITA-FKT 2002:01, 2002.
[18] M.S. Cheung, Y.K. Cheung, Natural vibrations of thin, flat-walled structures with different boundary conditions, *Journal of Sound and Vibration* 18 (1971) 325–337.
[19] M. Petyt, Finite strip analysis of flat skin-stringer structures, *Journal of Sound and Vibration* 54 (4) (1977) 537–547.
[20] D.J. Dawe, Use of the finite strip method in predicting the behaviour of composite laminated structures, *Composite Structures* 57 (2002) 11–36.
[21] F. Birgersson, S. Finnveden, A spectral super element for modelling of plate vibration. Part 2: turbulence excitation, *Journal of Sound and Vibration* 287 (2005) 315–328, this issue.
[22] M. Petyt, *Introduction to Finite Element Vibration Analysis*, Cambridge University Press, Cambridge, 1990.
[23] P.M. Morse, H. Feshbach, *Methods of Theoretical Physics*, McGraw-Hill, New York, 1953 (Chapter 3).
[24] F. Birgersson, Prediction of Random Vibration using Spectral Methods, PhD Thesis, MWL, KTH, 2004.
[25] J.T. Oden, *Mechanics of Elastic Structures*, McGraw-Hill, New York, 1967.
[26] F. Birgersson, Modelling with the Dynamic Stiffness and the Spectral Finite Element Methods for Distributed Sources, MSc Thesis, ISVR, The University of Southampton, 2000.
[27] F. Birgersson, N.S. Ferguson, S. Finnveden, Application of the spectral finite element method to turbulent boundary layer induced vibration of plates, *Journal of Sound and Vibration* 259 (2003) 873–891.